Giant and Nonanalytic Negative Piezoelectric Response in Elemental Group-Va Ferroelectric Monolayers

Shulin Zhong,[1] Xuanlin Zhang,[2] Shi Liu,[3,4] Shengyuan A. Yang[5] and Yunhao Lu[1,2,*]

[1]*School of Physics, Zhejiang University, Hangzhou 310027, Zhejiang Province, China*
[2]*State Key Laboratory of Silicon and Advanced Semiconductor Materials, School of Materials Science & Engineering,*
Zhejiang University, Hangzhou 310027, Zhejiang Province, China
[3]*Key Laboratory for Quantum Materials of Zhejiang Province, Department of Physics, School of Science,*
Westlake University, 600 Dunyu Road, Hangzhou 310030, Zhejiang Province, China
[4]*Institute of Natural Sciences, Westlake Institute for Advanced Study, 18 Shilongshan Road,*
Hangzhou 310024, Zhejiang Province, China
[5]*Research Laboratory for Quantum Materials, IAPME, Faculty of Science and Technology,*
University of Macau, Macau SAR, China

Materials with negative longitudinal piezoelectric response have been a focus of recent research. So far, reported examples are mostly three-dimensional bulk materials, either compounds with strong ionic bonds or layered materials with van der Waals interlayer gaps. Here, we report the first example in two-dimensional elemental materials—the class of group-Va monolayers. From first-principles calculations, we show that these materials possess giant negative longitudinal piezoelectric coefficient e_{11}. Importantly, its physical mechanism is also distinct from all previous proposals, connected with the special buckling driven polarization in these elemental systems. As a result, the usually positive internal strain contribution to piezoelectricity becomes negative and even dominates over the clamped ion contribution in Bi monolayers. Based on this new mechanism, we also find several 2D crystal structures that may support negative longitudinal piezoelectricity. As another consequence, piezoelectric response in Bi monolayers exhibits a significant nonanalytic behavior, namely, the e_{11} coefficient takes sizably different values (differed by $\sim 18\%$) under tensile and compressive strains, a phenomenon not known before and helpful for the development of novel electromechanical devices.

Piezoelectrics are materials which can convert mechanical energy into electrical energy and vice versa. They have found wide applications, e.g., in pressure sensors, actuators, and noise attenuators [1–3]. The performance of piezoelectrics is characterized by the piezoelectric response tensor. The longitudinal elements of the tensor e_{ii}, which measure the change of electric polarization along applied strain direction, are usually positive, because intuitively a tensile (compressive) strain should increase (decrease) the separation between positive and negative charges, and hence enhance (suppress) the polarization. Negative longitudinal piezoelectricity (NLP) was thought to be rare for a long time, although examples like poly (vinylidene fluoride) (β-PVDF) do exist [4–5]. The mechanism of NLP in β-PVDF was found to be complicated [6–10], likely connected to its quasi-1D polymer chain structures as well as complex dynamics of intermixed crystalline lamellae and amorphous regions [11]. Recently, there is a surge of interest in exploring materials with negative piezoelectricity. Theoretically, a number of three-dimensional (3D) bulk materials were predicted to host NLP, such as hexagonal ABC ferroelectrics [12], bismuth tellurohalides [13], HfO_2 [14], and some layered ferroelectrics [15]. Experimentally, NLP has

been detected in layered $CuInP_2S_6$ via *in situ* dynamic x-ray diffraction measurements [16].

In the meantime, there has been tremendous interest in 2D piezoelectric materials, due to their high crystallinity, free of dangling bonds, and ability to withstand enormous strain, which offer great flexibility in constructing various van der Waals (vdW) heterostructures with clean interface and tolerance of large lattice mismatch [17]. Up to now, several 2D ferroelectric and piezoelectric materials have been identified [18–21]. A recent proposal suggested that NLP should widely occur in layered ferroelectrics with out-of-plane polarization, a mechanism relying on the existence of vdW interlayer gaps to absorb most of the structural change [13,15–16]. Although 2D layers may be obtained from exfoliation of vdW layered materials, clearly, this mechanism cannot hold in the 2D monolayer limit due to the absence of any vdW gap here. Then, is there any new mechanism that can generate NLP in 2D monolayer materials?

In this Letter, we address the question above by revealing large NLP in a class of 2D *elemental* materials, the group-Va (As, Sb, Bi) monolayers. These 2D materials have been synthesized by physical vapor deposition and/or

molecular beam epitaxy methods [22–24]. Previously, they were predicted to be the first elemental ferroelectric materials [25]. Very recently, the ferroelectricity of Bi monolayer was confirmed in experiment [26]. Here, based on first-principles calculations, we uncover that these fascinating 2D materials also host significant NLP. The magnitude of e_{11} for Bi monolayer can reach over -1000 pC/m (~ -2.8 C/m² if converted to 3D unit). The mechanism for NLP here is also distinct from previous proposals. The ferroelectricity in these systems is the result of a special buckling distortion, which is directly affected by applied in-plane strain, such that the usually positive internal-strain contribution to piezoelectric response becomes negative here. In Bi monolayers, the negative internal-strain contribution can even dominate over the clamped ion contribution (which is also negative), leading to pronounced NLP. In addition, we report a previously unknown phenomenon: the nonanalyticity of piezoelectric response, namely, the (negative) piezoelectric coefficient differs for tensile and compressive strains. In 2D Bi, this difference can reach ∼18%. We show that this exotic effect is also a result of the buckling-driven mechanism, which determines anharmonicity of potential energy surface and different structural stiffnesses under stretch and compression. Our work extends the NLP effect to elemental materials, reveals a new NLP mechanism, and finds a novel nonanalytic behavior in piezoelectric response. These results may have important implications on functional materials design and device applications.

As illustrated in Fig. 1(a), the group-Va monolayers As, Sb, and Bi considered here all take the anisotropic α-phase structure, consisting of two buckled atomic layers, with four atoms in a primitive unit cell. The structure is similar to that of black phosphorene. The key difference is in the out-of-plane atomic buckling Δz [marked in lower panel of Fig. 1(a)] [25]. For black phosphorene, there is no buckling,
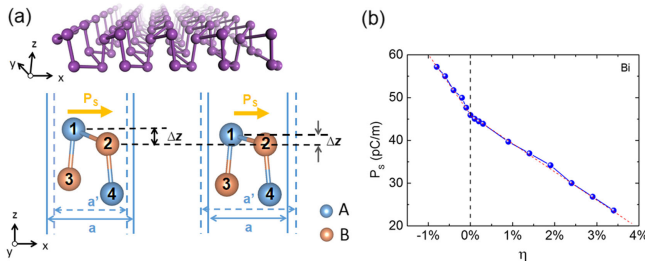

FIG. 1. (a) Top panel: crystal structure of 2D ferroelectric elemental group-Va monolayers (As, Sb, Bi). The spontaneous electric polarization P_s results from the atomic layer buckling, denoted as Δz in the lower panel. The polarization is in plane, along the x direction as in our setup. a is the equilibrium lattice constant and a' is the lattice constant under strain. The atoms are colored according to the sign of the net charge at the site. Sublattice A (B) acts like anions (cations). (b) Calculated polarization of Bi monolayer as a function of applied strain η along x axis. The slope corresponds to e_{11}.

i.e., $\Delta z = 0$, and its structure is nonpolar with preserved centrosymmetry [27]. Here, the finite buckling Δz breaks the centrosymmetry, reduces the symmetry to a polar group ($Pmn2_1$), and causes charge transfer between two sublattices [marked as A and B in Fig. 1(a)], forming cations and anions and leading to spontaneous in-plane polarization along the armchair direction [25], which is labeled as the x direction in Fig. 1(a). The detailed structural parameters obtained from our density functional theory (DFT) calculations are given in Table S1 of Supplemental Material (SM [28]) (detailed calculation methods are also presented in SM [28]). This buckled crystal structure has been confirmed for Sb and Bi monolayers in several experiments by scanning tunneling microscopy (STM) technique [23,26,37]. The calculated spontaneous polarization P_S values at equilibrium for As, Sb, Bi monolayer are 35, 32, 44 pC/m, respectively, which is also consistent with previous studies and recent experimental finding [25–26,38].

The piezoelectric tensor e_{ij} measures how the electric polarization changes under an applied strain, or equivalently, how the material is strained under an applied E field. In this study, we focus on the longitudinal piezoelectric coefficient e_{11}, which can be evaluated by

$$e_{11} = \frac{\partial P_S}{\partial \eta},$$

where η is the uniaxial strain applied along the x direction (i.e., along the axis of polarization).

In fact, based on the understanding of the special buckling-driven polarization in these group-Va 2D materials, we can naturally expect the appearance of NLP, before doing any calculation. For example, under a tensile strain $\eta > 0$ along x, since the atoms are strongly bonded as in Fig. 1(a) (i.e., the change of each bond length is small), one can easily see that the buckling height Δz should decrease under the stretch. This decrease of buckling moves the system toward the centrosymmetric structure, hence must suppress the electric polarization P_S, which then corresponds to NLP with $e_{11} < 0$. Similarly, for compressive strains, it should increase Δz and hence P_S, again leading to NLP.

This expectation is confirmed by our DFT calculation. The obtained e_{11} for the three group-Va monolayers are listed in Table I. For comparison, we also calculate the result for monolayer GeS, which is a well-studied 2D ferroelectric [39]. We find that group-Va monolayers indeed host large NLP. The values of e_{11} for As and Sb are -640 and -441 pC/m, and for Bi, it shows different values for stretch and compression, with $e_{11} = -866$ pC/m for $\eta > 0$ and $= -1020$ pC/m for $\eta < 0$ [see Fig. 1(b), we will discuss this nonanalytic behavior later]. These values are in fact quite significant. For example, if we convert the results for Bi monolayer to 3D unit, they are ~ -2.40 C/m² ($\eta > 0$) and -2.83 C/m² ($\eta < 0$), which are comparable or even

TABLE I. Theoretical values for the considered 2D monolayer materials (GeS is added for reference purpose). The meaning of the symbols is explained in the main text. The unit for piezoelectric coefficients is pC/m. For Z_{11}^* and $\partial u_1/\partial \eta$, the values for the two atomic sites in one sublattice (i.e., 1 and 4, 2 and 3) are the same. Meanwhile, for Z_{13}^* and $\partial u_3/\partial \eta$, the values for the two atomic sites in one sublattice have opposite signs, which is also indicated in Figs. 2(c) and 2(f).

	GeS	As	Sb	Bi ($\eta > 0$)	Bi ($\eta < 0$)
$e_{11}^{(0)}$	-113	-518	-378	-133	-59
$e_{11,x}^{(i)}$	930	-88	-49	-393	-383
$e_{11,z}^{(i)}$	-77	-34	-14	-340	-578
e_{11}	740	-640	-441	-866	-1020
$Z_{11}^*(1,\ 4)$	2.84	-0.44	-0.38	-1.69	-1.69
$Z_{11}^*(2,\ 3)$	-2.84	0.44	0.38	1.69	1.69
$(\partial u_1/\partial \eta)(1,\ 4)$	0.188	0.116	0.090	0.164	0.160
$(\partial u_1/\partial \eta)(2,\ 3)$	-0.188	-0.116	-0.090	-0.164	-0.160
$Z_{13}^*(1/4)$	$-1.08/1.08$	$1.06/-1.06$	$0.89/-0.89$	$1.70/-1.70$	$1.70/-1.70$
$Z_{13}^*(2/3)$	$0.62/-0.62$	$0.31/-0.31$	$0.18/-0.18$	$1.51/-1.51$	$1.51/-1.51$
$(\partial u_3/\partial \eta)(1/4)$	$-0.029/0.029$	$-0.008/0.008$	$-0.003/0.003$	$-0.044/0.044$	$-0.070/0.070$
$(\partial u_3/\partial \eta)(2/3)$	$0.017/-0.017$	$-0.001/0.001$	$-0.009/0.009$	$-0.025/0.025$	$-0.048/0.048$

larger than the well-known piezoelectrics such as ZnO [40] and AlN (wurtzite) [41].

To analyze piezoelectric response, the common practice is to decompose piezoelectric coefficient (e_{11} here) into two contributions: the clamped-ion contribution ($e_{11}^{(0)}$) and the internal-strain contribution ($e_{11}^{(i)}$) [42,43]. The clamped-ion contribution is evaluated at zero internal strain, i.e., when the fractional coordinates of the ions are frozen. It manifests the effect of redistribution of electrons and hence the change of Born effective charge under homogenous strain. The internal-strain contribution, on the other hand, captures the internal relaxation of ionic positions under strain, with the Born effective charges fixed. Considering the M_y mirror symmetry of the group-Va monolayers, the internal-strain contribution contains two terms $e_{11,x}^{(i)}$ and $e_{11,z}^{(i)}$. Therefore, we may write

$$e_{11} = e_{11}^{(0)} + e_{11,x}^{(i)} + e_{11,z}^{(i)}, \tag{1}$$

where

$$e_{11,x}^{(i)} = \frac{qa}{\Omega} \sum_n Z_{11}^*(n) \frac{\partial u_1(n)}{\partial \eta},$$

$$e_{11,z}^{(i)} = \frac{qc}{\Omega} \sum_n Z_{13}^*(n) \frac{\partial u_3(n)}{\partial \eta},$$

q is the electron charge, a and c are the lattice parameters along x and z, Ω is the unit cell area, index n runs over all ions in the cell, Z_{ij}^* is the Born effective charge tensor, and u_i is the fractional coordinate in the i th direction. The calculated values of the different contributions are summarized in Table I.

In a recent work, Qi and Rappe pointed out that the clamped-ion is generically negative due to the "lag of Wannier center" effect [15], whereas the internal-strain contribution is often positive. This feature is reflected in the results for 2D GeS in Table I. Thus, to achieve NLP, the previously proposed strategies are focused on enhancing the clamped-ion contribution and making it dominate over the internal-strain term. For example, this scenario can be achieved in ferroelectrics with strong ionic bonds such as the hexagonal ABC ferroelectrics [12]. Another possibility is vdW layered ferroelectrics with out-of-plane polarization, where the internal-strain contribution can be very small, since vdW gaps can accommodate most of the applied strain. Clearly, the group-Va monolayers here are distinct from those cases. As an elemental material, it is strongly covalently bonded and there are no weak bonds in the structure. This distinction is also manifested in the results in Table I. One observes that besides the clamped-ion contribution, the internal-strain contribution is also sizably negative for group-Va monolayers. Especially, for Bi, $e_{11}^{(i)}$ even dominates over (more than 5 times larger than) $e_{11}^{(0)}$, which is quite unusual.

Now we take a closer look at the three terms in Eq. (1) for group-Va monolayers. First of all, the negative clamped-ion term $e_{11}^{(0)}$ manifests the generic "lag of Wannier center" effect. Under a homogenous tensile strain $\eta > 0$, the factional coordinates of the ions are fixed (in the stretched unit cell). The change in Born effective charges can also be described in terms of the shift of Wannier center. In the paraelectric phase (i.e., $\Delta z = 0$), the Wannier center coincides with the ionic center. In the ferroelectric phase, the Wannier center deviates from the center of positive charge and moves in the $-x$ direction as in Fig. 2(a), forming a spontaneous polarization along the $+x$ direction. When applying tensile strain to the lattice, we find that the
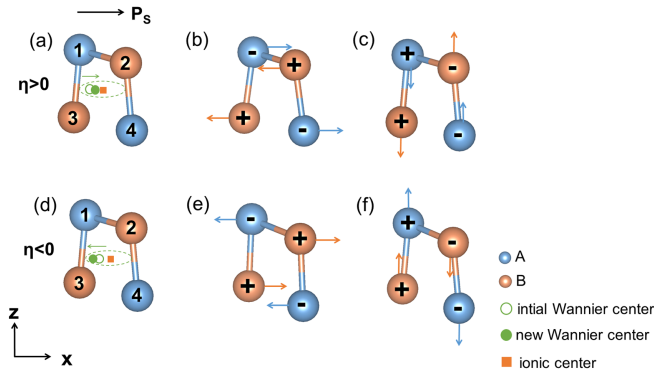
FIG. 2. Schematic illustration of the different contributions to NLP. The displacements of Wannier center and atomic positions are indicated for (a)–(c) $\eta > 0$ and (d)–(f) $\eta < 0$, respectively. The green dashed oval indicates the movement of the Wannier center at the clamped-ion state along the polar axis. The green solid circle and the hollow circle represent the new and the initial positions of the Wannier center, respectively. The orange solid square indicates the charge center of the ions. The blue and orange arrows indicate the moving direction of anions and cations when their positions are relaxed under strain. "+", "−" represent the sign of Born effective charges (see Table I).

FIG. 3. Potential energy surface along the x axis (in fractional unit of lattice constant a) and the z axis (in fractional unit of lattice constant c) for monolayer Bi under (a),(b) $\eta > 0$ and (c),(d) $\eta < 0$. Dashed lines represent the strain-free state and solid lines represent the clamped-ion state with a compressive or tensile strain of 1%. The corresponding clamped-ion (CI) and internal-strain (IS) contributions are marked by blue arrows.

Wannier center cannot completely follow the homogenous strain [see Fig. 2(a)]. It lags behind and hence has a relative shift along the polarization direction $(+P_S)$, which decreases the net polarization and leads to negative $e_{11}^{(0)}$. The sizable negative internal-strain terms $e_{11,x}^{(i)}$ and $e_{11,z}^{(i)}$ are connected to the buckled structure of these systems. In the ferroelectric phase, there is charge transfer between the two sublattices as shown in Fig. 2(b). The orange sites have net positive charges (cations) and the blue sites have negative changes (anions). Under a tensile strain, if allowing the internal relaxation of the ionic positions, we find that the ions would shift (from their initial fractional coordinates) along x and z as illustrated in Figs. 2(b) and 2(c), respectively. Regarding the horizontal shift, one observes that two sublattices move toward each other, which clearly decreases the net polarization P_S. In the meantime, the vertical shift moves the structure toward the centrosymmetric one, which also reduces P_S, as we discussed at the very beginning. Because of these, all the contributions to e_{11} are negative and hence lead to a significant NLP effect in these monolayer materials.

The different contributions can also be clearly visualized in the plot of potential energy surfaces (PESs) and polarizations versus the shift of atomic positions. As shown in Fig. 3(a), the dash (solid) lines are for Bi monolayers without strain (under 1% tensile strain). The black (red) colored lines are for PES (polarization). These quantities are plotted with respect to Δx, the displacement of the orange colored sublattice along the $+x$ direction, as illustrated in the inset of Fig. 3(a). In this plot, clearly, the difference between dashed and solid red lines at $\Delta x = 0$
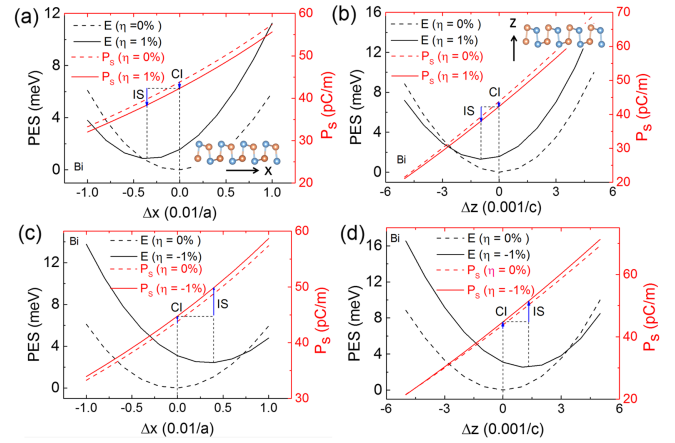
just corresponds to the clamped-ion contribution to the change in polarization at $\eta = 1\%$. Meanwhile, the minimum point $(\Delta x)_{eq}$ of PES corresponds to the equilibrium relaxed-ion state under a given strain. In Fig. 3(a), we find $(\Delta x)_{eq} < 0$ at $\eta = 1\%$, corresponding to a left shift of the red sublattice. At this point, the polarization is smaller than that at $\Delta x = 0$ in the strain-free state, and this difference just gives the internal-strain contribution due to horizontal relaxation. As shown in Fig. 3(a), both contributions are negative (indicated by the two blue arrows pointing downward), leading to NLP as expected. Similarly, Figs. 3(b)–3(d) show the results for compressive strain (-1%) and vertical sublattice displacement. The results for As and Sb monolayers are given in SM [28].

Finally, let us return to the unusual nonanalytic behavior for Bi monolayer as noticed before. As shown in Table I, both the clamped-ion term $e_{11}^{(0)}$ and the internal-strain term $e_{11,z}^{(i)}$ show obvious differences under tensile and compressive strains, but $e_{11,x}^{(i)}$ remain almost the same. This implies that the nonanalyticity should be closely related to buckling. As clarified in previous works [25], Bi has a weak hybridization between $6s$ and $6p$ orbitals, so that the bonds between Bi atoms are mainly determined by p orbitals, other than sp^3 configuration as in black phosphorene. As the Bi monolayer is extended in the x-y plane, the bonds are mainly contributed by p_x and p_y orbitals and the p_z electrons are left unpaired on one sublattice to form lone pairs of electrons, which tend to bring in the buckling (Δz) and drive the breaking of centrosymmetry (and hence electric polarization). The distribution of this lone-pair electron is sensitive to the energy difference of p_z levels on the two sublattices. Under small tensile strain, the energy
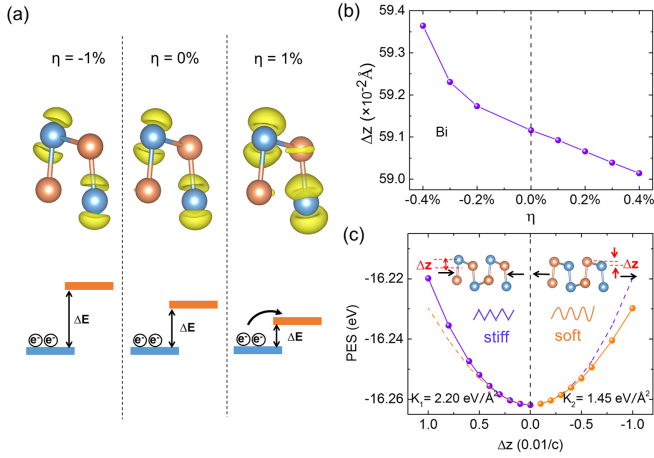
FIG. 4. (a) Projected charge densities of p_z orbital for Bi monolayer at three cases. (b) Buckling height Δz versus η for Bi monolayer. (c) Potential energy surfaces along z (in fractional unit of lattice constant c) for monolayer Bi. The dotted line is the polynomial fitting curve. K_2 and K_1 denote the stiffness coefficients extracted for $\Delta z < 0$ and $\Delta z > 0$, respectively.

splitting of p_z orbitals on two sublattices is reduced, resulting in charge redistribution and decreasing the charge transfer between the two sublattices [Fig. 4(a)]. In contrast, there is no obvious charge redistribution under small compressive strain, because the charge transfer already saturates. Since the charge redistribution is directly related to the shift of the Wannier center, it underlies the difference between the values of the clamped-ion term under tensile and compressive strains. The lone-pair electrons also affect the lattice distortion. Figure 4(b) shows the buckling height Δz of Bi monolayer as a function of η near equilibrium. It is noted that Δz under compressive (tensile) strain varies more rapidly (slowly) with η. This results in the different values of $e_{11,z}^{(i)}$. The jump in $e_{11,z}^{(i)}$ can also be understood from the anharmonicity of PES. In Fig. 4(c), we also draw the PES versus Δz. One can see that PES is anharmonic around the equilibrium point and the stiffness for $\Delta z < 0$ ($K_2 = 1.45$ eV/Å^2) is much less than that for $\Delta z < 0$ ($K_1 = 2.20$ eV/Å^2). Thus, it is easier to reduce Δz by tensile strain than increasing Δz by compressive strain. This can be intuitively understood from the above analysis of the difference in charge redistribution. In fact, the PESs for As and Sb also exhibit similar anharmonic features (shown in SM [28]). However, their internal-strain contributions are relatively small and hence the nonanalytic feature is not obvious in the overall e_{11}.

Discussion.—We have revealed a new mechanism for NLP. Essentially, it relies on a crystal structure in which the electric polarization is due to lattice buckling and the direction of buckling is normal to the polarization direction. It follows that when the material is stretched along the polarization direction, the buckling naturally decreases, hence the polarization decreases, leading to NLP. Based on

such understanding, we search through a 2D materials database [36] looking for materials (both elemental materials and compounds) with similar structural features. A list of materials which possess NLP are obtained. The screening process and the results are presented in SM [28].

In experiments, 2D materials usually need support by substrate. If choosing inert vdW layered materials as substrate (such as h-BN [44]), the substrate effect on the 2D material is usually very weak and properties like NLP discussed here should be preserved. On the other hand, one may also choose some stretchable substrate (like PDMS [45]) which has sizable interaction with the 2D material, such that strain applied by deforming the substrate can be detected as electric signals in the 2D NLP materials on top. This could be useful for sensor and electromechanical device applications.

*Corresponding author: luyh@zju.edu.cn
[1] R. M. Martin, Phys. Rev. B **5**, 1607 (1972).
[2] P. Shivashankar and S. Gopalakrishnan, Smart Mater. Struct. **29**, 053001 (2020).
[3] Z. L. Wang and J. H. Song, Science **312**, 242 (2006).
[4] H. Burkard and G. Pfister, J. Appl. Phys. **45**, 3360 (1974).
[5] H. Ohigashi, J. Appl. Phys. **47**, 949 (1976).
[6] S. M. Nakhmanson, M. B. Nardelli, and J. Bernholc, Phys. Rev. Lett. **92**, 115504 (2004).
[7] K. Tashiro, M. Kobayashi, H. Tadokoro, and E. Fukada, Macromolecules **13**, 691 (1980).
[8] Y. Wada and R. Hayakawa, Jpn. J. Appl. Phys. **15**, 2041 (1976).
[9] R. Kepler and R. Anderson, J. Appl. Phys. **49**, 4490 (1978).
[10] T. Furukawa, IEEE Trans. Electr. Insul. **24**, 375 (1989).
[11] I. Katsouras, K. Asadi, M. Li, T. B. Van Driel, K. S. Kjaer, D. Zhao, T. Lenz, Y. Gu, P. W. Blom, and D. Damjanovic, Nat. Mater. **15**, 78 (2016).
[12] S. Liu and R. E. Cohen, Phys. Rev. Lett. **119**, 207601 (2017).
[13] J. Kim, K. M. Rabe, and D. Vanderbilt, Phys. Rev. B **100**, 104115 (2019).
[14] J. Liu, S. Liu, J.-Y. Yang, and L. Liu, Phys. Rev. Lett. **125**, 197601 (2020).
[15] Y. Qi and A. M. Rappe, Phys. Rev. Lett. **126**, 217601 (2021).
[16] L. You, Y. Zhang, S. Zhou, A. Chaturvedi, S. A. Morris, F. Liu, L. Chang, D. Ichinose, H. Funakubo, W. Hu, T. Wu, Z. Liu, S. Dong, and J. Wang, Sci. Adv. **5**, eaav3780 (2019).
[17] A. K. Geim and I. V. Grigorieva, Nature (London) **499**, 419 (2013).
[18] H. Zhu, Y. Wang, J. Xiao, M. Liu, S. Xiong, Z. J. Wong, Z. Ye, Y. Ye, X. Yin, and X. Zhang, Nat. Nanotechnol. **10**, 151 (2015).

[19] J. Xiao, H. Zhu, Y. Wang, W. Feng, Y. Hu, A. Dasgupta, Y. Han, Y. Wang, D. A. Muller, L. W. Martin, P. Hu, and X. Zhang, Phys. Rev. Lett. **120,** 227601 (2018).

[20] F. Liu, L. You, K. L. Seyler, X. Li, P. Yu *et al.*, Nat. Commun. **7,** 12357 (2016).

[21] K. Chang, J. Liu, H. Lin, N. Wang, K. Zhao, A. Zhang, F. Jin, Y. Zhong, X. Hu, W. Duan, Q. Zhang, L. Fu, Q.-K. Xue, X. Chen, and S.-H. Ji, Science **353,** 274 (2016).

[22] P. J. Kowalczyk, S. A. Brown, T. Maerkl, Q. Lu, C.-K. Chiu, Y. Liu, S. A. Yang, X. Wang, I. Zasada, F. Genuzio *et al.*, ACS Nano **14,** 1888 (2020).

[23] Q. Lu, J. Cook, X. Zhang, K. Y. Chen, M. Snyder, D. T. Nguyen, P. V. S. Reddy, Bi. Qin, S. Zhan, L.-D. Zhao, P. J. Kowalczyk, S. A. Brown *et al.*, Nat. Commun. **13,** 4603 (2022).

[24] Y. Lu, W. Xu, M. Zeng, G. Yao, L. Shen, M. Yang, Z. Luo, F. Pan, K. Wu, T. Das, P. He, J. Jiang, J. Martin, Y. P. Feng, H. Lin, and X.-S. Wang, Nano Lett. **15,** 80 (2015).

[25] C. C. Xiao, F. Wang, S. A. Yang, Y. Lu, Y. Feng, and S. Zhang, Adv. Funct. Mater. **28,** 1707383 (2018).

[26] J. Gou, H. Bai, X. Zhang, Y. L. Huang, S. Duan, A. Ariando, S. A. Yang, L. Chen, Y. Lu, and A. T. S. Wee, Nature (London) **617,** 67 (2023).

[27] L. Li, Y. Yu, G. J. Ye, Q. Ge, X. Ou, H. Wu, D. Feng, X. H. Chen, and Y. Zhang, Nat. Nanotechnol. **9,** 372 (2014).

[28] See Supplemental Material at http://link.aps.org/supplemental/10.1103/PhysRevLett.131.236801 for additional details of the calculations and the monolayer structure of As, Sb, and Bi, negative piezoelectric response of As and Sb, the results of different functional and SOC effect for calculations, PES of As and Sb, workflow and results of the high-through calculations, which includes Refs. [29–36].

[29] G. Kresse and J. Hafner, Phys. Rev. B **47,** 558 (1993).

[30] J. P. Perdew, K. Burke, and M. Ernzerhof, Phys. Rev. Lett. **77,** 3865 (1996).

[31] P. E. Blöchl, Phys. Rev. B **50,** 17953 (1994).

[32] H. J. Monkhorst and J. D. Pack, Phys. Rev. B **13,** 5188 (1976).

[33] K. A. D. R. Jiří, J. Phys. Condens. Matter **22,** 022201 (2010).

[34] D. Vanderbilt and R. D. King-Smith, Phys. Rev. B **47,** 1651 (1993).

[35] R. Resta, Rev. Mod. Phys. **66,** 899 (1994).

[36] J. Zhou, L. Shen, M. D. Costa, K. A. Persson, S. P. Ong, P. Huck, Y. Lu, X. Ma, Y. Chen, H. Tang, and Y. P. Feng, Sci. Data **6,** 86 (2019).

[37] T. Nagao, J. T. Sadowski, M. Saito, S. Yaginuma, Y. Fujikawa, T. Kogure, T. Ohno, Y. Hasegawa, S. Hasegawa, and T. Sakurai, Phys. Rev. Lett. **93,** 105501 (2004).

[38] F. M. Xu, H. Su, Z. Gong, Y. Wei, H. Jin, and H. Guo, Phys. Rev. B **106,** 195418 (2022).

[39] R. Fei, W. Li, L. Ju, and Y. Li, Appl. Phys. Lett. **107,** 173104 (2015).

[40] X. Wu, D. Vanderbilt, and D. R. Hamann, Phys. Rev. B **72,** 035105 (2005).

[41] F. Bernardini and V. Fiorentini, Phys. Rev. Lett. **79,** 3958 (1997).

[42] G. Sághi-Szabó, R. E. Cohen, and H. Krakauer, Phys. Rev. Lett. **80,** 4321 (1998).

[43] S. de Gironcoli, S. Baroni, and R. Resta, Phys. Rev. Lett. **62,** 2853 (1989).

[44] W. Yang, G. Chen, Z. Shi, C.-C. Liu, L. Zhang, G. Xie, M. Cheng, D. Wang, R. Yang, D. Shi, K. Watanabe, T. Taniguchi, Y. Yao, Y. Zhang, and G. Zhang, Nat. Mater. **12,** 792 (2013).

[45] K. S. Kim, Y. Zhao, H. Jang, S. Y. Lee, J. M. Kim, K. S. Kim, J.-H. Ahn, P. Kim, J.-Y. Choi, and B. H. Hong, Nature (London) **457,** 706 (2009).